Banana rachis-based biochar in situ impregnated with Zn-based compounds: effect of the precursor concentration on characteristics, adsorbent and antibacterial capacity

Rimaycuna J.[1], Cruz J.F.[2], Matějová L.[3], Solis R.L.[1], Solis J.L.[5], Kuśtrowski P.[6], Gomez M.M.[7], Martaus A.[3], Cruz G.J.F[1*]

[1]Grupo de Investigación "Aprovechamiento de biomasa residual agroindustrial para diversas aplicaciones", Universidad Nacional de Tumbes, Campus Universitario s/n Barrio Pampa Grande, Tumbes, Perú
[2]Departamento de Química – Facultad de Ingeniería de Minas, Universidad Nacional de Piura, Campus Universitario s/n Urbanización Miraflores, Piura, Perú
[3]Institute of Environmental Technology, Centre for Energy and Environmental Technologies, VSB-Technical University of Ostrava, 17.istopadu 15/2172, 708 00 Ostrava-Poruba, Czech Republic
[4]Facultad de Ciencias, Universidad Nacional de Ingeniería, Av Tupac Amaru 210, Rimac, Lima, Peru
[5]Faculty of Chemistry, Jagiellonian University, Gronostajowa 2, 30-387 Krakow, Poland

*****Corresponding author: gcruzc@untumbes.edu.pe

Banana rachis-based biochar in situ impregnated with Zn-based compounds: effect of the precursor concentration on characteristics, adsorbent and antibacterial capacity

Rimaycuna J.[1], Cruz J.F.[2], Matějová L.[3], Solis R.L.[1], Solis J.L.[4], Kuśtrowski P.[5], Gomez M.M.[4], Martaus A.[3], Cruz G.J.F[1*]

[1]1Grupo de Investigación "Aprovechamiento de biomasa residual agroindustrial para diversas aplicaciones", Universidad Nacional de Tumbes, Campus Universitario s/n Barrio Pampa Grande, Tumbes, Perú
[2]Departamento de Química – Facultad de Ingeniería de Minas, Universidad Nacional de Piura, Campus Universitario s/n Urbanización Miraflores, Piura, Perú
[3]Institute of Environmental Technology, Centre for Energy and Environmental Technologies, VSB-Technical University of Ostrava, 17.istopadu 15/2172, 708 00 Ostrava-Poruba, Czech Republic
[4]Facultad de Ciencias, Universidad Nacional de Ingeniería, Av Tupac Amaru 210, Rimac, Lima, Peru
[5]Faculty of Chemistry, Jagiellonian University, Gronostajowa 2, 30-387 Krakow, Poland

*****Corresponding author: gcruzc@untumbes.edu.pe

Abstract

Biochar is an adsorbent material widely used to remove pollutants from water and wastewater. However, biochars have limited adsorption capacity for some pollutants and antibacterial properties, therefore enriched with functional groups from different compounds such as Zn-based ones. In that sense, this research aimed to impregnate Zn-containing NPs onto banana rachis-based biochar using the in situ wet method with zinc nitrate heptahydrate (ZnN) as precursor. The effect of different concentration of ZnN (0.5, 1 and 2 M) on impregnated biochar properties, adsorption capacity and antibacterial capacity were evaluated. Zn-containing compounds such as residual ZnN, $Zn_5(NO_3)_2(OH)_8 \cdot 2H_2O$ (ZHN) and/or ZnO, mostly in the crystalline phase, were deposited on the biochar surface, incorporating surface functional groups such as NO_3 and Zn-O, mainly. When the lowest initial precursor concentration was used, ZnN is predominant in the crystalline phase, while when the concentration of the precursor increased the main compound is ZHN. The incorporation of oxygenated surface functional groups increased Pb and brilliant blue adsorption capacities of the impregnated materials compared to the bare biochar. However, within the impregnated biochars, the increased precursor concentration causes a reduction in the adsorption capacity because of the obstruction of microporosity. The impregnation enhanced the antibacterial capacity of biochar against bacteria. The antibacterial capacity increases with the enlarged precursor concentration, and it is based on Zn^{2+} releasing. Impregnation of biochar with ZnN using mild post-impregnation temperature conditions improved the adsorption and antibacterial capacities. Nevertheless, further studies should be carried out with other kinds of pollutants.

Keywords: Zn-based compound, Zinc nitrate concentration, banana rachis-biochar, adsorption, antibacterial capacity

1.- Introduction

Water pollution is a hotspot environmental issue worldwide. Severe water pollution episodes have had placed in different parts of the world, including Latin America where the legislation and the governmental inspection is still a relevant challenge. Peru is one of the most important exporters of mining commodities in South America, being water pollution a critical environmental problem [1, 2]. According to the Technical Water Quality Monitoring Reports of the Peruvian Water Authority, most water sources do not comply with the environmental quality standards for water. In previous works [3, 4] one of the pollution episodes in Tumbes, northwest of Peru, has been explained. Illegal mining in Ecuador releases heavy metals in the bi-national river Puyango-Tumbes. Pb^{2+} is widely reported in Tumbes River water and sediments [5, 6], being potential hazard for human health. Pb^{2+} is the second most toxic element, after As^{5+}, having the ability to be accumulated in the food chain and causing different magnitude of human health negative effects [7].

Dyes are another common pollutant family found in different effluents released from food, textile, pharmaceutical industries [8-10], among other. Blue brilliant (BB) is an anionic dye that is poisonous to the respiratory tract, as well as carcinogenic and mutagenic [11]

Due to the risks associated with the presence of contaminants in the aquatic environment, more efforts are being made to develop treatment technologies that can effectively remove the toxic elements [12]. Adsorption on biochars is a powerful and environmentally friendly technology for water treatment. Biochar can be produced using a wide range of abundant and low-cost raw material using pyrolysis under inert gases (nitrogen, argon, etc.). It is a material with a low toxicity and with surface area and favorable surface chemistry for adsorption processes [13]. However, biochar can be also modified to improve their adsorption properties or to incorporate new features such as photocatalytic activity, antibacterial properties [14], and supercapacitor activity.

ZnO in form of nanoparticles (NPs) is the most frequently used Zn-based compound for impregnation of biochar. Recent studies have demonstrated the improved properties of biochar/ZnO for removal/degradation of contaminants [12, 14-18]. Besides, the antibacterial capacity of biochar/ZnO, alone or combine with other compounds, has been

demonstrated against ATCC bacteria including *Escherichia coli* and *Staphylococcus aureus* [19].

One of the methods used for ZnO NPs impregnation is the *in situ* wet precipitation method by zinc nitrate hexahydrate as a precursor [20, 21] followed by a thermal treatment to form ZnO NPs. However, under drastic thermal treatment the formation of other Zn-containing compounds is inevitable. Previous studies have demonstrated the formation of ZnO as higher calcination temperature is applied, nevertheless as pure ZnO NPs [22, 23]. In the case of in situ impregnation of biochar, heating in oxygen or air environments could affect the original biochar properties. Additionally, the influence of the precursor concentration on the characteristics of impregnated materials and the adsorption and antibacterial properties has not been completely dilucidated. Besides ZnO, other Zn-containing compounds can be deposited on biochar surface derived mainly from the reactions of the precursor during impregnation process, even more when mild conditions are applied after impregnation process. The Zn-containing compounds different from ZnO affect the material properties and could affect the ability of the materials to adsorb pollutants and its antibacterial properties. On the other hand, the antibacterial activities of biochar/ZnO have been demonstrated in relation to Gram-positive and Gram-negative bacteria [24]. Nevertheless, there is a lack of information about antibacterial properties of these materials in relation to bacteria isolated from real wastewater, which could have antibacterial resistance. In this context, the aim of this study wasto evaluate the effect of impregnation with different $Zn(NO_3)_2 \cdot 6H_2O$ concentrations on the properties of biochar, the formation of Zn-based compounds and adsorption properties. Antibacterial capacity between produced materials and to ZnO NPs as positive control has been compared.

2.- Material and methods

2.1.- Biomass sampling and conditioning

Banana rachis was collected in San Jacinto district - Tumbes region – northwest of Peru. 50 kg of banana rachis was collected from the main banana packaging companies in the area. Residual biomass was cleaning with abundant potable water to remove particles from the material surface. Then, it was dried in an oven (*Memmert* SNB 400) at 100 °C until constant weight was reached. The dried material was ground and sieved to obtain particle size fraction between 0.5 – 1 mm. The final material was stored in plastic bags until biochar production.

2.2.- Formation and modification of biochar

Biochar was obtained using a procedure conducted in previous research [14, 25]. Briefly, ground, and sieved biomass was put in a reactor located in a tubular horizontal oven (*Nabertherm GmbH,* Alemania). The material was carbonized at 600 °C during 2 h in an inert nitrogen flux (150 mL/min). The reactor was cooled, and the material was repeatedly washed with an acid solution (HCl 0.1 N) and distilled water. Finally, the biochar was dried at 80 °C until constant mass and then sieved to reach particle size less than 0.25 mm.

For the impregnation of biochar with the ZnO NPs, the *in situ* wet precipitation method was conducted with zinc nitrate hexahydrate (ZnN) as the precursor. Biochar was mixed and constantly stirred in a NaOH solution (proportion 1/10 m/V). The dispersion was heated until 60 °C and the aqueous solution of ZnN was titrated drop by drop. Three different concentrations of the ZnN solution were used, namely 0.5, 1.0 and 2.0 M. After the titration, the mixture was stirred for 30 min. The biochar impregnated was recovered and repeatedly washed with distilled water. Finally, the impregnated biochars were dried in an oven at 70 °C for 12 h. The produced bare biochar and biochar/ZnO were named as BW-B for the bare banana rachis biochar (biochar without ZnO), whereas BW-ZnN0.5, BW-ZnN1 and BW-ZnN2 for biochar impregnated using the 0.5 M, 1 M and 2 M precursor solution, respectively.

2.3.- Adsorbents characterization

2.3.1. Proximate, ultimate, and elemental analyses

Moisture and ash contents were determined by gravimetric analyses using ASTM methods [26, 27]. The analyses of fixed carbon and volatile components (wt.%) were performed according to the ASTM D7582 standard using a TGA 701 thermogravimetric analyser (LECO, USA). The ultimate analysis to determine C, H, and N in wt.% was done by using a CHNS 628 (LECO, USA) analyser according to the ASTM D3172-13 and D5373-16 standards.

Semiquantitative determination of chemical elemental composition including Si, P, K, Ca, Fe and Zn was carried out using X-ray fluorescence (XRF) spectrometry measured on a XEPOS energy dispersion spectrometer (Spectro, Germany). Zn^{2+} concentration (in wt.%) in biochars was determined in a ContrAA 700 atomic absorption spectrometer (AAS) (Analytik Jena, Germany), using an optical system and working in complete wavelength range (185 – 900 nm). It was equipped with a monochromator with a double diffraction

grating and a Xenon short-arc lamp. The flame technique was applied. For analysis, adsorbents were previously digested with concentrated HNO_3.

2.3.2. Surface characterization

X-ray photoelectron spectroscopy (XPS) measurements were carried out on a Prevac system equipped with a hemispherical VG SCIENTA R3000 analyzer and a monochromatized aluminum source AlK_α (1486.6 eV). The pass energy was fixed at 100 eV. Binding energies in the collected spectra were calibrated using the C 1s line at 284.8 eV. Gaussian-Lorentzian peak fitting was conducted after a Shirley background subtraction in the Casa XPS software.

The functional groups on the biochar surface were analyzed using a Fourier transform infrared (FTIR) spectrum analyzer (Thermo Nicolet 360 FTIR E.S.P. Spectrometer, USA). Raman spectra were recorded using a μ-Raman system with high resolution focal (LabRAM HR800- Horiba, Japan), with solid-state laser excitation (638 nm).

The pH of zero charge (pH_{PZC}) was measured using the pH drift method. 0.01 M potassium nitrate (KNO_3) solution was prepared and saturated with nitrogen gas to reduce the effect of CO_2. 50 mL of the solution was placed into 8 Erlenmeyer flasks (200 mL). In every flask, the pH level was adjusted to reach pH values between 3 and 10 using 0.1 N solutions of NaOH and H_2SO_4. 0.1 g of biochar and functionalized biochar were added to each Erlenmeyer, sealed, and placed under constant stirring for 48 h in an orbital shaker (Geselischaft für Labortechnik, Germany). Then, aliquots of each Erlemeyer were taken and filtered with Whatman 1 filter paper and the final pH was determined with a Sentix 940-3 potentiometer. The pH_{PZC} was calculated from the intercept of the initial pH vs final pH curves.

2.3.3 Structural properties

The crystalline structure of the adsorbents was studied by X-ray powder diffraction (XRD) using a SmartLab diffractometer (Rigaku, Japan) operated at 40 kV and 40 mA, C_oK_α radiation (λ = 0.179278 nm). X-ray diffraction patterns were collected in the range of 5° to 90° 2Θ. The analysis and interpretations of the XRD patterns for crystalline phases were done using PDXL 2 software (version 2.4.2.0, Rigaku, Japan) and compared with database PDF-2, release 2015 (ICDD, USA).

2.3.4 Textural properties

The textural characteristics of the biochar-based materials were determined measuring N_2 physisorption at 77 K using a 3Flex adsorption volumetric apparatus (Micromeritics, USA). Prior to the physisorption experiment, the biochar-based materials were degassed at ~0.05-0.1 mbar vacuum at 350 °C for 2 days to release physisorbed water and residual surface-bonded volatiles. Using the adsorption data of the measured N_2 adsorption-desorption isotherm, the specific surface area (S_{BET} in m^2/g) was determined according to the standard Brunauer-Emmett-Teller (BET) method for the pressure range p/p_0 = 0.05-0.25. The net pore volume (V_{net} in cm_{liq}^3/g) was calculated from the N_2 volume adsorbed at the maximum relative pressure of p/p_0=0.99. Since all biochar-based materials are microporous solids, the micropore volume (V_{micro} in cm_{liq}^3/g) and the mesopore surface area (S_{meso} in m^2/g) were calculated using the t-plot method and carbon black STSA standard isotherm. The mesopore-size distribution was evaluated from the adsorption branch of the isotherm using the Barret-Joyner-Halenda (BJH) method, carbon black STSA standard isotherm and assumption of the slit-pore geometry (characterized with the pore width w_p). The micropore-size distribution was evaluated from the adsorption branch of the isotherm at $p/p_0 \sim 1 \cdot 10^{-9}$-0.05 using the Horwath-Kawazoe solution for the slit-pore geometry (also characterized with the pore width w_p). Since the open hysteresis was reached during physisorption measurements on some biochar-based materials, the adsorption branch of the N_2 adsorption-desorption isotherm was used for pore-size distribution evaluations.

2.4. Adsorption experiments

2.4.1. BB adsorption experiments

Brilliant blue (BB) dye equilibrium and kinetic experiments were conducted for the produced adsorbents. For the equilibrium experiments, a standard solution of 1 000 mg/L of BB (Merck, USA) was prepared, and then solutions of 5, 10, 20, 50, 100, 200 and 250 mg/L were obtained with the pH adjusted to 6. This pH was determined in previous preliminary experiments as the optimal level of adsorption of the dye. 150 mL of each solution was placed in flasks and 0.15 g of the produced materials (particle size less than 0.25 mm) was added to be placed in orbital shaking for 48 h at 30 °C. Then, aliquots were taken, filtered, and analyzed in a Lambda 365 UV-VIS spectrophotometer (Perkin Elmer, USA) at 664 nm. To evaluate the equilibrium adsorption data, the nonlinear form of

Langmuir, Freundlich and Dubinin-Radushkevich models were used.

For the kinetic experiments, 10, 20, 50 and 100 mg/L BB solutions were prepared, and the pH was adjusted to 6. 200 mL batch solutions were used for the experiments and 0.2 g of the produced biochars (particle size less than 0.25 mm) was added. The biochars were placed under stirring for 240 min in a multi-stirrer 15 magnetic stirrer (Velp Scientifica, Italy). Aliquots at 0, 2, 5, 10, 15, 20, 30, 60, 90, 120, 180 and 240 min were taken and filtered through Whatman 1 filter paper, and the liquid phase was analyzed in the UV-VIS spectrophotometer. To evaluate the kinetic adsorption data, the non-linear form of pseudo-first order (PFO) and pseudo-second order (PSO) models were applied. Additionally, the intraparticle diffusion model were used to analyze the adsorbent transport mechanism.

2.4.2. Pb adsorption experiments

Similar to BB dye, Pb equilibrium and kinetic tests were conducted. For the equilibrium tests, Pb (Sigma-Aldrich Corporation, USA) solutions of 10, 20, 50, 100 and 200 mg/L with the pH adjusted between 5 – 6 were used. 100 mL of solutions were put in flasks and 0.03 g (particle size less than 0.25 mm) of the produced adsorbents was added. The flask was constantly shacked during 48 h at 30°C in an orbital shaker. After that, 10 mL aliquots were collected, filtered, and preserved with 150 µl of concentrated nitric acid. Pb concentration was measured using the AAS technique. To analyze the equilibrium adsorption data, the nonlinear form of Langmuir, Freundlich and Dubinin-Radushkevich models were used.

In the case of the Pb kinetic experiments, solutions of 10, 50 and 100 mg/L of Pb were used. 100 mL of solution with the pH adjusted to 6 and two doses of the synthetized materials were used 0.03 and 0.05 g. Flasks were placed under stirring for 240 min in a multi-stirrer 15 magnetic stirrer and aliquots were periodically collected at 0, 2, 5, 10, 15, 20,30, 60, 90, 120, 180 and 240 min. The aliquots were filtered through Whatman 1 filter paper and preserved with 150 µL of concentrated nitric acid, and then measured using AAS. To analyze the Pb kinetic adsorption data, the non-linear form of pseudo-first order (PFO) and pseudo-second order (PSO) models were applied. Additionally, the intraparticle diffusion model were used to study the adsorbent transport mechanism.

2.5.-Antibacterial activity

The antibacterial activity of the produced biochars was investigated against three Gram

negative strains (*Proteus vulgaris*, *Citrobacter freundi* and *Escherichia coli*) and one Gram positive strain (*Bacillus firmus*). Bare ZnO NPs were used as positive control. The bacterial strains were isolated from wastewater, and they are part of the Molecular Biology Laboratory's strain collection, National University of Tumbes. The modified Kirby-Bauer method [28] was applied. The bacteria strains were cultured in tryptic soy broth (TSB) for 24 h at 37°C, then they were centrifuged to obtain pellets, which were washed 3 times with sterile physiological saline solution, followed by centrifugation. The clean pellet was resuspended in sterile physiological saline solution to achieve an optical turbidity comparable to tube number 0.5 of the Mc Farland scale (OD_{600}=0.08-0.1), with an approximate cell density of 1.5×10^8 CFU/mL. Optical density was measured in a Lambda 365 UV-VIS spectrophotometer (Perkin Elmer, USA). Afterwards, 100 µL of the bacteria was inoculated on the surface of a Petri dish containing tryptic soy agar (TSA). Subsequently, with the help of a clamp, a cylinder of 6 mm diameter was placed in the center of the plate and 0.02 and 0.04 g of the produced materials or ZnO NPs were placed inside. Finally, the cylinders were removed, and the petri dishes were incubated for 24 h at 37 °C in a F260-PLUS incubator (Memmert, Germany). The presence of an inhibition zone around the biochar demonstrated the inhibition of microorganisms. The diameter of the inhibition zone was measured in mm.

3. Results and discussion

3.1 Materials characterization

3.1.1 Proximate, ultimate, and elemental analyses

Table 1 shows the results of proximate (moisture, ash and fixed C), ultimate (C, H, N and S) and elemental (Si, P, K, Ca and Fe) composition of the produced adsorbents.

The moisture content in the bare biochar (BW-B) was 8.0%, while for the impregnated materials this parameter increased as the concentration of the precursor ZnN increased (9.8%, 10.3% and 12.7% for BW-ZnN0.5, BW-ZnN1, BW-ZnN2 respectively). It could be due to the higher amount of ZnN during impregnation results in the increasing of hydrophobic sites on the biochar surface. Related to the ash content, the tendency is similar to the moisture case, this parameter increased as the concentration of the precursor ZnN increased (27.7%, 67.5%, 71.2% and 82.9% for BW-B, BW-ZnN0.5, BW-ZnN1 and BW-ZnN2, respectively). Obviously, the increase in the ash content is related to raising amount of the minerals compound remained on the biochar surface when the ZnN loading is

increased.

The proximate analysis of bare biochar and modified biochars evidences that the impregnation process of biochar contributes to the increase in the volatiles content and decrease in the fixed carbon content. The reduction in fixed carbon content proportion is a result of increasing Zn-based compounds concentration after impregnation.

The ultimate analysis (Table 1) shows that the N content increases with the increasing amount of ZnN precursor (), indicating the presence of residual not-decomposed NO_3^- in the ZnO-modified biochars. On contrary, the C content decreases with raising ZnN concentration, because of the increasing in mineral compounds in ash content.

From the elemental analyses (Table 1), Zn is the only element that significantly increases with the ZnN precursor concentration. The Zn content was measured by XRF and AAS, and similar results were obtained for both methods.

Table 1. Results of proximate, ultimate, elemental analyzes (wt%) and surface composition (atomic ratios) of investigated adsorbents

Parameter	BW-B	BW-ZnN0.5	BW-ZnN1	BW-ZnN2
Proximate analysis (wt%)[a]				
Moisture	8.0	9.8	10.3	12.7
Ash	37.7	67.5	71.2	82.9
Volatile	20.0	29.0	39.6	62.0
Fixed C	58.8	38.5	23.2	10.4
Ultimate analysis (wt%)[b]				
C	66.8	47.9	36.6	18.9
H	2.7	2.1	1.4	1.5
N	1.2	2.9	4.4	6.7
S	0.2	ND	0.1	0.2
Elemental analysis (wt%)[c]				
Ca	3.6	2.1	1.5	0.5
Cu	0.005	0.004	0.003	0.001
Fe	0.4	0.2	0.2	0.1
K	6.4	4.2	3.9	1.6
Mn	0.02	0.01	0.01	0.01
P	1.0	0.7	0.6	0.2
Si	1.7	1.6	1.3	0.5
Zn	0.02	9.1	13.7	18.0
Zn (AAS)	0.01	7.3	11.5	18.7
Surface composition (atomic ratios)[d]				
Zn/C	0.0	1.3	1.3	2.1
O/C	0.4	1.2	1.2	2.1

[a] moisture and ash were determined by gravimetric method and fixed C by TGA
[b] determined by elemental CHNS (C, H, N, S),
[c] determined by XRF, additionally Zn was detected by AAS
[d] determined by XPS
ND - Not detected

It is important to notice that K is an essential element in the case of banana culture and therefore its amount is very high in the biochars, taking the highest concentration of 6.4wt% for BW-B. The K concentration is reduced as increasing of ZnN concentration during impregnation. The same effect occurs in the case of other elements such as Ca, Cu, Fe, Mn, P, and Si.

3.2.2 Structural properties

The crystalline structure of the prepared adsorbents was studied by X-ray powder diffraction (XRD). As shown in the XRD patterns (Figures 1a and b and Table 2) all adsorbents exhibit two wide bands centered at 2θ=27.8° and 49.6°, which correspond to C(002) and C(100), respectively [29], and prove the existence of 2L amorphous carbon. The first diffraction peak is related to the amorphous structure of the carbon with randomly oriented aromatic sheets, whereas the second one is attributed to the graphitic structure of the carbon. However, in the case of BW-ZnN1 and BW-ZnN2 both peaks are not so clearly visible because of the appearance of many sharp features assigned to Zn-based crystalline phases.

Table 2. Phase composition of produced adsorbents

Adsorbent/ Phase composition	BW-B	BW-ZnN0.5	BW-ZnN1	BW-ZnN2
SiO_2	X	X	X	X
2L amorphous carbon	X	X	X	X
$Zn(NO_3)_2 \cdot 6H_2O$	ND	X	ND	ND
$Zn_5(NO_3)_2(OH)_8 \cdot 2H_2O$	ND	ND	X	X
ZnO	ND	ND	X	ND
Feldspars	X	ND	ND	ND

ND – not detected

In all produced adsorbents, a crystalline phase of quartz (SiO_2) was identified (PDF2 card no. 01-074-1811), since it is a natural component of the raw material (banana rachis) and comes from the soil and air dust. The elemental analyses indicated that the contents of Si in the adsorbents are 1.7, 1,6, 1.3 and 0.5 wt% for BW-B, BW-ZnN0.5, BW-ZnN1 and BW-ZnN2, respectively (Table 1). Additional peaks, which are not indexed in the BW-B XRD pattern, come from feldspars (part of the soil), including probably some minor crystalline phase(s) containing K, which, however, is not possible to exactly identify. The

presence of minor K-containing feldspars may be supported by the presence of high content of K in BW-B identified by XRF (6.4 wt%) (see Table 1). BW-ZnN0.5 contains besides crystalline SiO_2 also original crystalline Zn precursor $Zn(NO_3)_2 \cdot 6H_2O$ (PDF2 card no. 00-046-0596). Contrary to that, BW-ZnN1 and BW-ZnN2 show the peaks of crystalline SiO_2, $Zn_5(NO_3)_2(OH)_8 \cdot 2H_2O$ (PDF2 card no. 00-024-1460) and ZnO (only BW-ZnN1) (PDF2 card no. 01-079-0207), which disclose slight oxidation of the original Zn precursor after its impregnation on bare BW-B due to drying at 70°C, forming those Zn-crystalline phases.

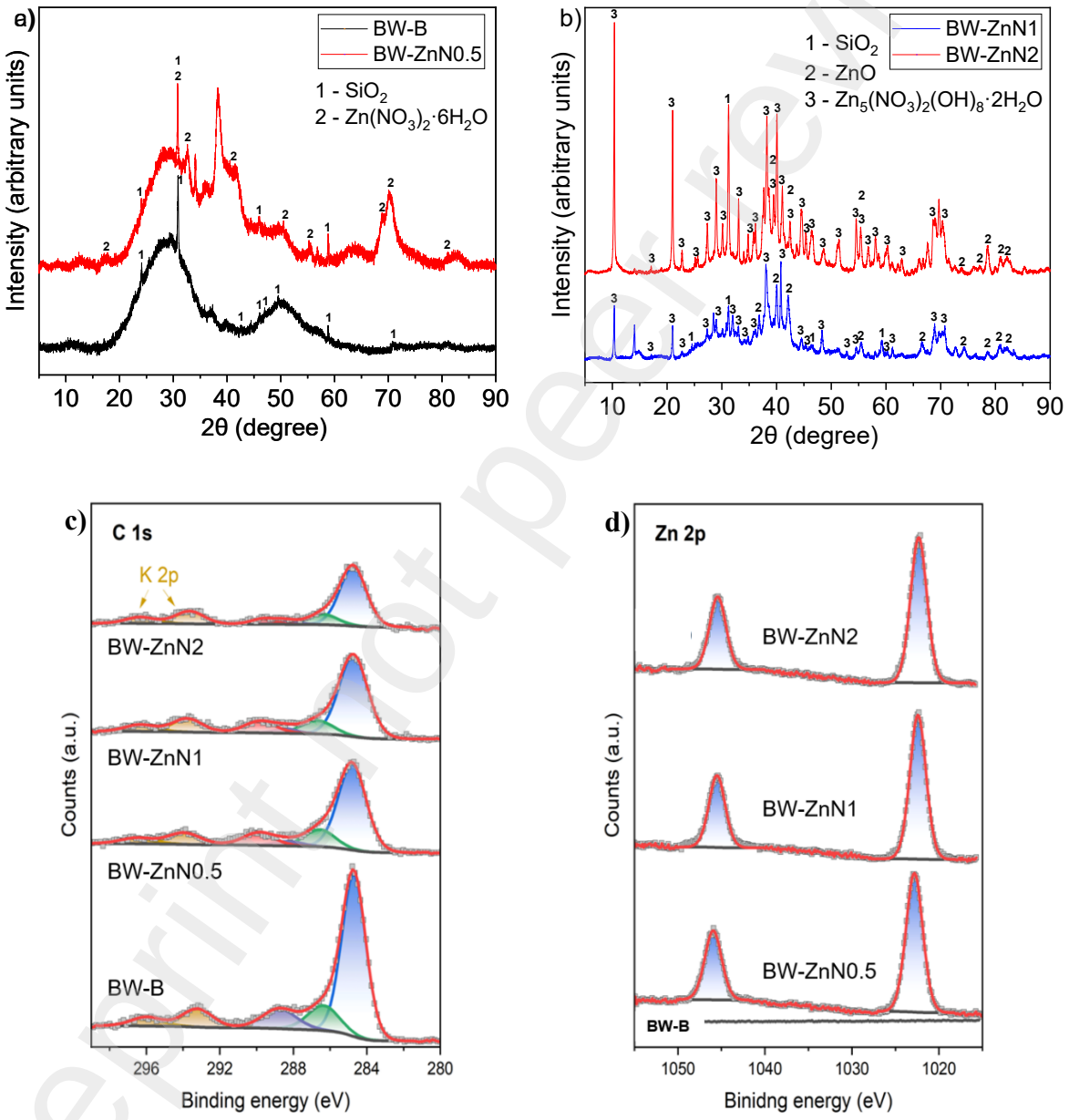

Figure 1. XRD patterns of produced adsorbents: BW-B and BW-ZnN0.5 (a), BW-ZnN1 and BW-ZnN2 (b). High-resolution XPS spectra of produced adsorbents recorded in C 1s (c) and Zn 2p (d) regions.

3.2.3 Surface properties

The surface composition of the banana rachis biochar before and after modification with various amounts of ZnN was examined by XPS. The results are shown in the form of deconvoluted XPS C 1s and Zn 2p spectra in Figure 1c and 1d respectively. Additionally, Table 1 presents the Zn/C and O/C atomic ratios determined based on the areas of the recorded XPS peaks after taking into account appropriate relative sensitivity factors. As expected, the pristine biochar exhibits a complex surface structure. The XPS C 1s spectrum of this material shows components related to the presence of C-C/C=C (at 284.8 eV), C-O (at 286.4 eV) and C=O (at 288.3 eV) species [30]. Furthermore, the material's surface contains quite a lot of oxygen species, as evidenced by the relatively high atomic ratio O/C = 0.4. However, it should be remembered that the hemispherical analyzer gains photoelectrons emitted by all forms of oxygen identified on the surface, including those originating from mineral impurities. For this reason, we have not decided to discuss the XPS O 1s spectrum. Its reliable deconvolution is practically impossible due to the rich composition of the surface of the studied biochar.

The modification of biochar results in the appearance of Zn-containing surface species. With raising concentration of Zn^{2+} nitrate used, the Zn/C atomic ratio in the final product increases and reaches a value as high as 2.1 for the BW-ZnN2 material. Because Zn is deposited in the form of oxygen-containing compounds, the O/C ratio increases simultaneously. However, it is worth paying attention to the characteristic doublet of Zn $2p_{1/2}$ and Zn $2p_{3/2}$ with the spin orbit splitting of 23.0-23.1 eV in the XPS Zn 2p spectra. The position of the Zn $2p_{3/2}$ peak changes gradually with the amount of Zn from 1022.8 eV (for BW-ZnN0.5) to 1022.3 eV (for BW-ZnN2.0). Such a high binding energy (E_b) in the case of BW-ZnN0.5 should be explained by the formation of surface $ZnCO_3$ or rather $Zn_5(OH)_6(CO_3)_2$ [31], which is also confirmed by the appearance of an additional peak in the XPS C 1s spectra at 289.8±0.1 eV attributed to C in carbonates. As crystallites of the surface Zn phase increases, the bulk fraction growths and therefore the Zn $2p_{3/2}$ peak shifts towards a lower E_b value characteristic of ZnO (~ 1022.1 eV).

In the XPS C 1s spectra (Figure 1c) it is possible to identify two peaks K $2p_{3/2}$ (293.2 eV) and K $2p_{1/2}$ (296.0 eV). As it was aforementioned, K is an element, which remains in the produced samples after processing of the raw material. Therefore, the intensities of both K peaks are more intense in the case of bare biochar.

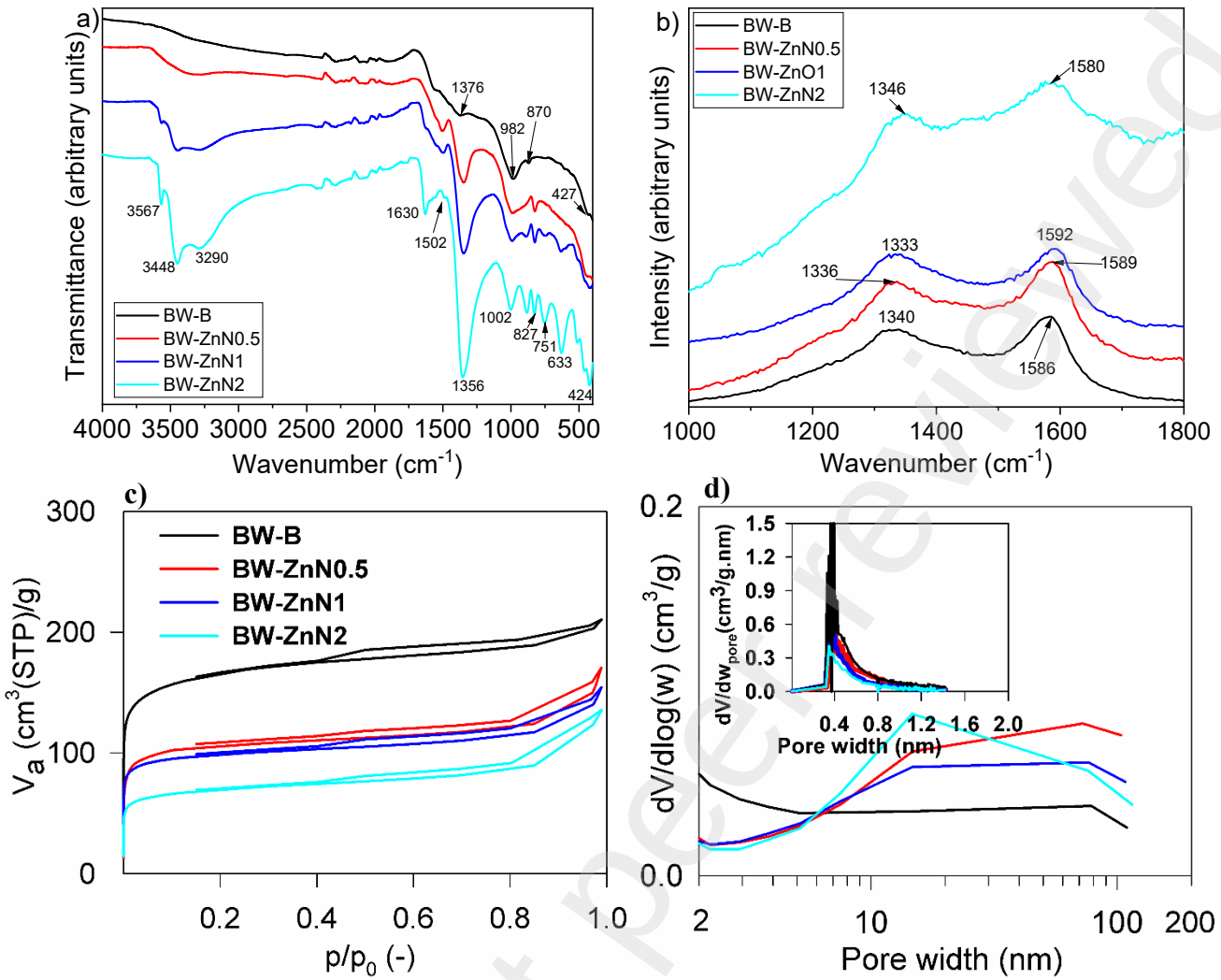

Figure 2. FTIR (a) and Raman (b) spectra of adsorbents. Measured nitrogen adsorption-desorption isotherms at 77 K (c), evaluated mesopore-macropore-size distributions (d) and evaluated micropore-size distributions (inset of d) of adsorbents.

The surface functional groups of the produced biochars detected by FTIR are shown in Figure 2a. BW-B presents bands at 1376, 982, 870 and 427 cm^{-1}, which correspond to H-O-H bending vibration [32], C-O [33] or C-C, C-H and Si-O bond, respectively. In the FTIR spectra region of structural vibrations, SiO_2 is identified as important component of the used biochar.

A wide band centered around 3340 cm^{-1} started to be visible in BW-ZnN0.5. This band become wider and more intense as the concentration of ZnN increased, additionally, the peak splits to two peaks 3565 and 3443 cm^{-1} in the case of BW-ZnN1 and to three peaks 3567, 3448 and 3290 for BW-ZnN2.

Others new bands also appear with the ZnN impregnation, even the intensity of those

increase with the increasing in the concentration of the precursor. The BW-ZnN0.5 spectrum shows bands at 1492, 1376, 982, 823 and 426 cm^{-1}; BW-ZnN1 at 1492, 1356, 991, 887, 824, 631, 512 and 423 cm^{-1}; while BW-ZnN2 at 1630, 1502, 1356, 1002, 882, 827, 751, 633, 512, 450 and 424 cm^{-1}. In general, the intensity of common peaks, in the impregnated biochars, growths as the initial concentration of the ZnN precursor increased, due to increasing Zn-compounds amount on the biochar surface.

For BW-ZnN0.5, the XRD analysis detected the crystalline phase of ZnN. Furthermore, the bands in the FTIR spectra of this material at 3340, 1376 and 823 cm^{-1} would correspond to ZnN [34, 35], coinciding with the XRD results. The bands at 1376 and 823 cm^{-1} are related to the vibrational modes of nitrate ion. XPS also revealed the presence of carbonate-based compounds in this material (BW-ZnN0.5). The peak at 1376 cm^{-1} could be also due to CO_3^{2-} of mineral carbonate [36, 37].

In the case of BW-ZnN1 and BW-ZnN2, zinc hydroxide nitrate (ZHN) was detected by XRD. The FTIR spectrum of BW-ZnN2 is similar to that of ZNH discussed by other authors [38, 39]. The strong peaks at 3567 cm^{-1} and 3448 cm^{-1} as well as a shoulder peak at 3290 cm^{-1} would correspond to OH group vibrations, while peaks between 1002-827 cm^{-1} to nitrate group [40]. Additionally, the presence of both bands at 3290 and 1630 cm^{-1} would indicate the presence of water molecules in the interlayer space and/or absorbed on the surface [39]. The FTIR spectrum of BW-ZnN1 also discloses the bands at 1356 cm^{-1} and between 991-824 cm^{-1} related to the presence of ZHN.

The band between 424 - 426 cm^{-1}, identified in the impregnated biochars, partially correlates with the SiO_2, also detected in the bare biochar by XRD. However, the peak is more intense and/or wider in the case of impregnated materials compared to BW-B. It is well known that the peaks close to this wavenumber are assigned to the vibrations of Zn-O bonds in ZnO NPs [32, 41, 42]. In the case of BW-ZnN1 the ZnO phase was detected by XRD and XPS.

Summarizing, the additional functional groups in the impregnated biochar compared to the bare one include nitrates and/or CO_3^{2-}.

Raman spectra (Figure 2b) indicate more differences in surface and structural characteristics between the bare biochar and the modified biochars. The spectrum of the bare biochar shows bands at 1340 and 1586 cm^{-1}, assigned as D and G bands, typically present in this kind of carbonized materials. As it is well known, the D band is referred to sp^3-hybridized carbon atoms, which is associated with amorphous structure, while the G

band corresponds to sp^2-hybridized carbon atoms, i.e. crystalline structure of the material [16]. The Raman spectra of the impregnated biochars present both bands, but with different intensity, as observed in Figure 2b. Calculating the ratio I_D/I_G for the materials, it was obtained 0.856, 0.863, 0.966 and 0.905 for BW-B, BW-ZnN0.5, BW-ZnN1, BW-ZnN2 respectively. Higher I_D/I_G ratio indicates a higher level of structural disorder and defects, while a lower ratio is related to fewer defects and a more ordered structure. BW-B and BW-ZnN0.5 contain more ordered carbon structure than the biochars impregnated with higher amount of ZnN (BW-ZnN1 and BW-ZnN2). This is due to the higher concentration of Zn-based compounds deposited on the structure of those two materials.

The pH of point of zero charge (pH_{PZC}) values for the produced materials were 8.74, 7.12, 6.95 and 6.85 for BW-B, BW-ZnN0.5, BW-ZnN1, BW-ZnN2 respectively. Clearly, the modification of biochar reduces the pH_{PZC}. It indicates that the impregnation process modified the surface of the biochars, in such a way that the point at which the net surface charge is equal to zero is reduced. Similar reduction in the pH_{PZC} was observed in a previous study [14] when ZnN was used for impregnation of biochars.

3.2.4 Textural properties

Figure 2 c, d and inset of d depict the N_2 adsorption-desorption isotherms at 77 K and evaluated mesopore-macropore-size and micropore-size distributions of the produced adsorbents, respectively. According to the IUPAC classification [43] the isotherms of all produced adsorbents correspond to the combination of isotherm type I and IV with the H4-type hysteresis loop. This combined isotherm type corresponds to microporous origin of adsorbents containing also wide range of mesopores and macropores. From Figure 2c it is visible that for BW-ZnN0.5 a BW-ZnN1 the open hysteresis was reached during physisorption measurements. This open hysteresis may be attributed to following phenomena: (i) the leakage of some residual volatiles condensed in smaller mesopores from pyrolysis or impregnation process and/or (ii) some change of carbon structure, both in a consequence of evacuation/pressure decrease accompanying the N_2 desorption measurement. This open hysteresis is very often typical for biochars and it may indicate incomplete biomass carbonization as well.

Table 3. Textural properties of produced adsorbents

Biochar	Specific surface area S_{BET} (m^2/g)	Mesopore surface area S_{meso} (m^2/g)	Micropore volume V_{micro} (cm_{liq}^3/g)	Net pore volume V_{net} (cm_{liq}^3/g)
BW-B	560	79	0.225	0.325
BW-ZnN0.5	335	47	0.144	0.263
BW-ZnN1	314	43	0.133	0.238
BW-ZnN2	224	48	0.087	0.210

The determined textural properties, such as the specific surface area, mesopore surface area, net pore volume and micropore volume, are summarized in Table 3. The parent BW-B biochar shows the best textural parameters, while the textural properties of the impregnated adsorbents are getting worst with increasing amount of Zn-precursor impregnated. ZnO and other Zn-based phases formed/crystallized due to their impregnation are placed on the mesoporous-macroporous surface of the bare biochar, plugging partially entrance of micropores and, thus, reducing the micropore volume from 0.225 (for BW-B) to 0.087 cm_{liq}^3/g (for BW-ZnN2) as well as external mesopore surface area from 79 m^2/g (for BW-B) to 43-48 m^2/g (for Zn-doped biochars). As a consequence of this phenomena the net pore volumes also decreased (from 0.325 cm_{liq}^3/g for BW-B to 0.210-0.263 cm_{liq}^3/g for Zn-doped biochars). Mesopore surface areas of Zn-doped biochars stay more or less comparable 43-48 m^2/g. Concerning the pore-size distributions (Fig. 2d and inset of 2d), it is affected with present Zn-based phases and their micro/structural properties (phase composition, crystal sizes). But it is evident, concerning the micropore-size distributions (inset of Figure 2d), they are identical for all adsorbents, just decreasing the peak intensity corresponding to decreasing micropore volume with increasing Zn precursor loading. Concerning the mesopores-macropore-size distribution, they are also identical and there exist wide range of mesopores and macropores in adsorbents with pore diameter in the range of 7-100 nm.

3.3 Brilliant blue (BB) Adsorption Experiments

3.3.1 Equilibrium adsorption experiments

Figures 3 shows the data and adjustment of BB adsorption isotherms to the Langmuir, Freundlich and Dubinin-Radushkevich models. Figures 3a, 3b, 3c and 3d depict results for materials BW-B, BW-ZnN0.5, BW-ZnN1 and BW- ZnN2, respectively. It is evident that

the impregnated biochars almost reach the equilibrium, while BW-B does not reach it at the experimental conditions.

Table 4 shows the experimental parameters for the applied non-linear models to determine the best one that fits the BB dye adsorption equilibrium. Considering the comparison of the correlation coefficients (R^2) and the chi-square statistic (X^2), the BW-B adsorption data fits the best to the Freundlich model, following by the Langmuir and Dubinin-R models. The data for BW-ZnZ0.5 fits the best to the Langmuir model, closely following by the Dubinin R model; BW-ZnZ1 to the Freundlich model, closely following by Dubinin R model; and finally, BWZnN2 to the Dubinin-R model, following by the Freundlich model. However, analyzing the Freundlich model fitted curves (red curves in Figure 3), the slope of those curves tends to be increased when C_e is higher without reaching equilibrium. While the Dubinin-R model fitted curves tend to maintain the equilibrium. According to these facts, the Dubinin-R model is considered to compare the equilibrium adsorption parameters of the materials. In that sense, the impregnated biochars show better maximum equilibrium adsorption (q_{DR}), being the order from higher to lower: BW-ZnN0.5 > BW-ZnN1 > BW-ZnN2 ~ BW-B.

The adsorption energy (E), determined by the Dubinin R model, is related to the type of mechanism that takes place during adsorption: physical (E <8 kJ/mol), ion exchange (E = 8–16 kJ/mol) or chemical (E= 20-200 kJ/mol) [44]. In the case of the produced materials, BW-B and BW-ZnN0.5 are in the range of physical adsorption, while BW-ZnZ1 and BW-ZnZ2 are typical of ion exchange. Additional functional oxygenated groups on the surface of the impregnated biochars (NO_3^- and Zn-O) would favor the interaction with a higher number of BB dye molecules, increasing the E value. However, the reduction in the textural properties as the increase in the ZnN concentration during impregnation caused an opposite effect.

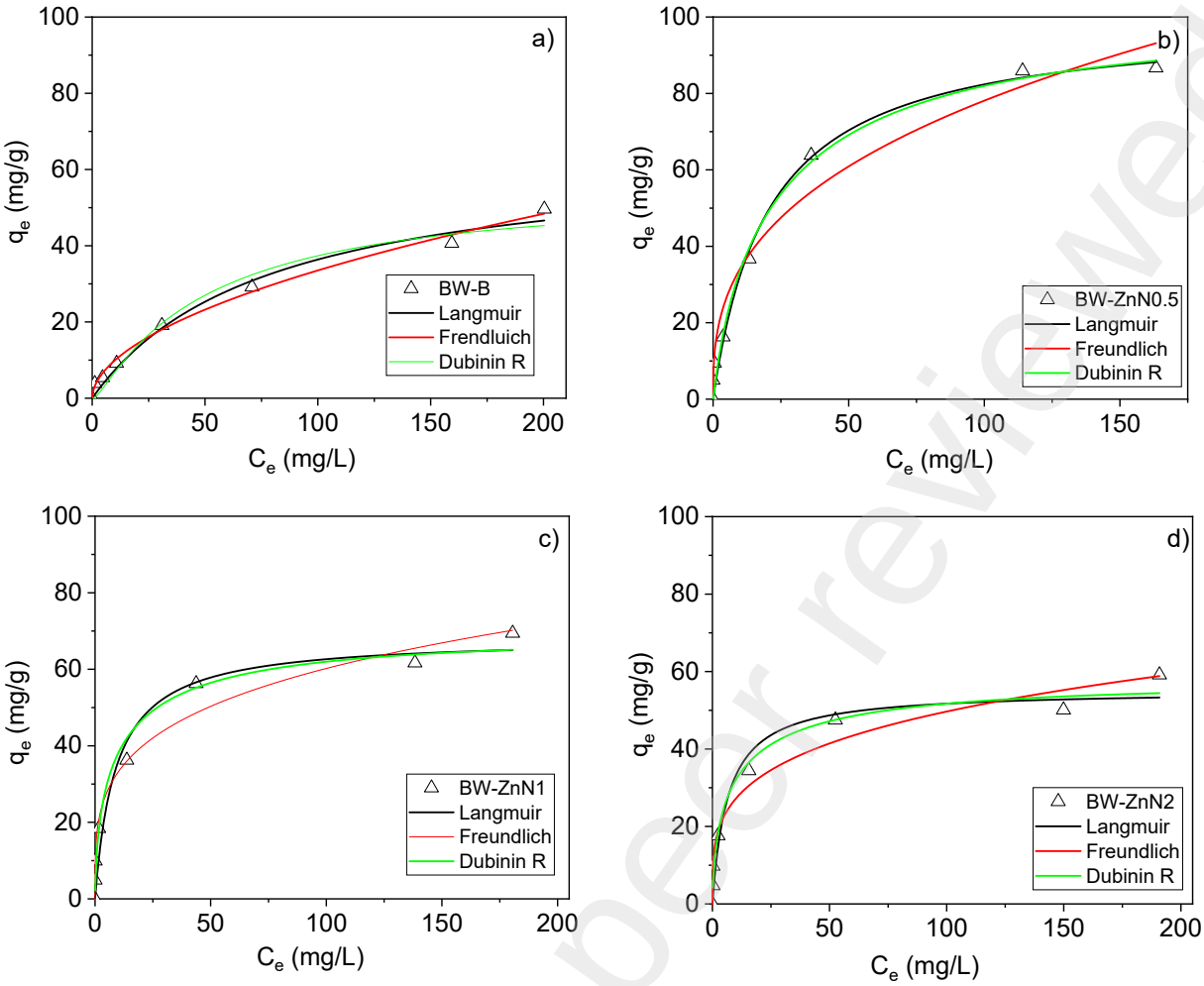

Figure 3. BB dye adsorption isotherms (303 K) of the materials, BW-B (a), BW-ZnN0.5 (b), BW-ZnN1 (c) and BW-ZnN2 (d).

Table 4. Non-linear models fitted for BB equilibrium adsorption data.

Models	Parameters	BW-B	BW-ZnN0.5	BW-ZnN1	BW-ZnN2
Langmuir	Qmax (mg/g)	64.75	99.32	68.30	55.13
	K_L (L/g)	0.012	0.048	0.110	0.150
	R^2	0.986	0.991	0.958	0.962
	X^2	5.64	14.19	36.99	23.33
Freundlich	K_F (mg/g) /(mg/L)^n	2.93	14.95	18.25	14.87
	N	0.52	0.35	0.25	0.26
	R^2	0.995	0.976	0.982	0.970
	X^2	2.10	36.88	15.98	18.22
Dubinin-Radushkevich	qDR(mg/g)	52.74	98.16	68.41	56.97
	K_{DR} (mol^2/kJ^2)	0.026	0.013	0.007	0.007
	E (kJ/mol)	4.38	6.20	8.45	8.45
	R^2	0.975	0.990	0.978	0.982
	X^2	9.87	14.84	19.59	10.72

3.3.2 Kinetic adsorption experiments

The kinetic experiments were carried out in a batch reactor, using the produced materials with a particle size of >0.25 mm, pH = 6, biochar dose of 1 g/L, and periodically withdrawn aliquots in a total time of 240 min. Figure 4 depicts the BB kinetic adsorption data of the materials collected at different initial adsorbate concentrations 10, 20, 50 and 100 mg/L (Figure 4a, b, c and d respectively). In all cases, the impregnated biochars showed better kinetic adsorption behavior compared to the bare biochar. All materials with different initial BB concentrations reach the equilibrium in the first 30-60 min, nevertheless the level of equilibrium varies for the impregnated biochars. When the initial BB concentration was 10 mg/L, the impregnated biochars showed almost similar kinetic adsorption behavior. However, when the initial BB concentration increased, the difference in kinetic adsorption behavior of the impregnated materials is more evident, being in order of higher to lower: BW- ZnN-0.5 > BW-ZnN1 > BW-ZnN2.

Despite textural properties of BW-B are better than those for impregnated materials, the functional groups formed after the impregnation process interact with the BB molecules, allowing higher adsorption. However, when the concentration of ZnN was increasing during the impregnation process, the pores in the biochar were partially blocked. Higher concentration of ZnN reduced the surface area and the number of active sites capable of BB adsorption.

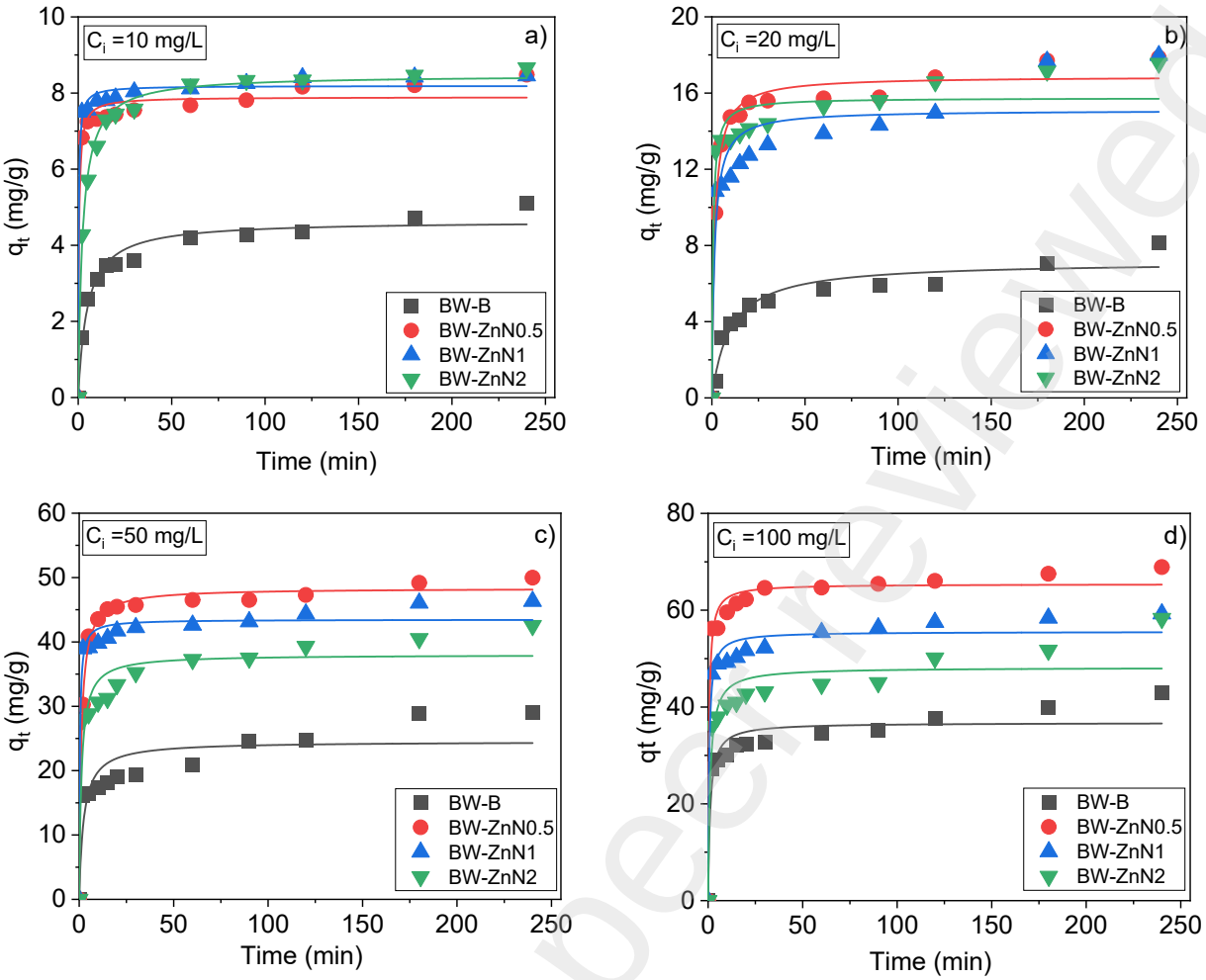

Figure 4. BB dye kinetic adsorption curves of the produced materials at initial concentration of 10 (a), 20 (b), 50 (c) and 100 mg/L (d).

Table 5 shows the experimental parameters of the nonlinear models applied to the kinetic BB adsorption data. Analyzing R^2 and X^2 for the models, the pseudo-second order model, in all cases, fits the best to BB kinetic data. The q_e parameter of pseudo-second order model is higher in the case of the impregnated biochars compared to the bare material, considering all the initial BB concentration tested. BB is an anionic dye, mainly because of its three negatively charged sulfonic acid groups. Based on the pH value of BB solutions (pH=6.0) during adsorption experiments and the pH_{PZC} of the adsorbents, the net surface charge of the produced materials would be positive. Thus, the BB adsorption by the produced materials is favored under these conditions. Therefore, BW-B (pH_{PZC}=8.74) presents more positively charge surface than the impregnated materials BW-ZnN0.5 (7.12), BW-ZnN1 (6.95) and BW-ZnN2 (6.85). Evidently, as higher the concentration of the precursor during impregnation, lower the pH_{PZC} and weaker the positively surface charge.

Table 5. Parameters of models fitted for BB dye kinetic adsorption data at different initial concentrations.

Models	Parameters	BW-B	BW-ZnN0.5	BW-ZnN1	BW-ZnN2
		C_i =10 mg/L			
Pseudo-first order	q_1(mg/g)	4.29	7.73	8.07	7.99
	k_1(min^{-1})	0.14	1.05	1.30	0.27
	R^2	0.907	0.971	0.986	0.950
	X^2	0.21	0.15	0.08	0.33
Pseudo- Second order	q_e (mg/g)	4.64	7.89	8.19	8.47
	k_2(g/mg.min)	0.04	0.32	0.48	0.05
	R^2	0.969	0.982	0.992	0.993
	X^2	0.06989	0.09682	0.04641	0.04090
Intraparticle diffusion	k_{Diff1} (mg/g $min^{-0.5}$)	1.01	4.83	5.30	3.02
	R_1^2	0.981	1	1	1
	k_{Diff2} (mg/g $min^{-0.5}$)	0.21	0.15	0.13	0.81
	R_2^2	0.944	0.836	0.836	0.977
	k_{Diff3} (mg/g $min^{-0.5}$)	0.12	0.09	0.05	0.09
	R_3^2	0.944	0.949	0.891	0.803
		C_i =20 mg/L			
Pseudo-first order	q_1(mg/g)	6.45	16.08	14.15	15.20
	k_1(min^{-1})	0.08	0.41	0.58	0.91
	R^2	0.898	0.959	0.798	0.912
	X^2	0.62	1.07	4.64	2.01
Pseudo- Second order	q_e (mg/g)	7.14	16.87	15.10	15.74
	k_2(g/mg.min)	0.01	0.04	0.05	0.10
	R^2	0.944	0.985	0.872	0.943
	X^2	0.34	0.39	2.95	1.32
Intraparticle diffusion	k_{Diff1} (mg/g $min^{-0.5}$)	1.13	4.78	7.66	9.18
	R_1^2	0.940	0.933	1	1
	k_{Diff2} (mg/g $min^{-0.5}$)	0.18	0.41	0.50	0.35
	R_2^2	0.948	0.825	0.951	0.990
	k_{Diff3} (mg/g $min^{-0.5}$)	0.47	0.26	0.146	0.19
	R_3^2	0.998	0.894	1	1
		C_i =50 mg/L			
Pseudo-first order	q_1(mg/g)	22.37	46.56	42.62	35.99
	k_1(min^{-1})	0.43	0.49	1.19	0.62
	R^2	0.719	0.984	0.969	0.873
	X^2	18.04	3.43	5.32	17.26
Pseudo- Second order	q_e (mg/g)	24.53	48.35	43.47	38.02
	k_2(g/mg.min)	0.02	0.02	0.07	0.02
	R^2	0.826	0.995	0.981	0.935
	X^2	11.16	1.07	3.28	8.80
Intraparticle diffusion	k_{Diff1} (mg/g $min^{-0.5}$)	11.46	18.61	27.53	19.74
	C_1 (mg/g)	$-1.25x10^{-15}$	1.06	$-2.51x10^{-15}$	$-2.51x10^{-15}$
	R_1^2	1	0.986	1	1
	k_{Diff2} (mg/g $min^{-0.5}$)	1.03	2.12	0.89	1.82
	C_2 (mg/g)	14.14	36.45	37.32	24.93
	R_2^2	0.977	0.949	0.949	0.974
	k_{Diff3} (mg/g $min^{-0.5}$)	0.12	0.41	0.40	0.70
	R_3^2	1	0.938	0.945	0.978
		C_i =100 mg/L			
Pseudo-first order	q_1(mg/g)	34.97	63.78	54.02	45.84
	k_1(min^{-1})	0.65	1.01	0.96	0.66
	R^2	0.87265	0.9668	0.9518	0.85566
	X^2	16.37	12.67	13.42	32.46
Pseudo- Second order	q_e (mg/g)	36.75	65.39	55.55	48.16
	k_2(g/mg.min)	0.03	0.03	0.03	0.02
	R^2	0.924	0.985	0.973	0.906
	X^2	9.78	5.77	7.56	21.18
Intraparticle diffusion	k_{Diff1} (mg/g $min^{-0.5}$)	19.21	39.74	33.09	25.43
	R_1^2	1	1	1	1
	k_{Diff2} (mg/g $min^{-0.5}$)	1.45	2.23	1.30	1.81
	R_2^2	0.927	0.968	0.951	0.956
	k_{Diff3} (mg/g $min^{-0.5}$)	1.01	0.45	0.95	1.49
	R_3^2	0.971	0.935	0.921	0.909

Table 5 shows the parameters of the intraparticle diffusion model, whereas Figure S1 depicts the adjustment of this model to the experimental data. The intraparticle diffusion model includes three steps, as following surface diffusion, intraparticle diffusion and equilibrium adsorption on an adsorbent surface. For almost all materials and experimental conditions those three steps are identified. The parameters indicate that the data fits well to the intraparticle model in every step. BB molecular size is around 1.07 nm×1.47 nm× 1.88 nm [45]. It means that a pore size-limiting effect to partially access microporosity of the materials could be observed. The k_{Diff1} (adsorption rate for surface diffusion step) values are higher for the impregnated biochars compared to the bare material. Even comparing between the impregnated materials, the tendency is similar to that explained previously (BW-ZnN-0.5 > BW-ZnN > BW-ZnN2). However, the values of k_{Diff2} (adsorption rate for intraparticle diffusion step) and k_{Diff3} (adsorption rate for equilibrium adsorption step) are variable, being in most of cases higher for the impregnated materials, but with a difference not as high as in the case of k_{Diff1}. It means that the higher adsorption capacity of the impregnated biochars compared to the bare one takes place during the surface diffusion step. Despite the impregnated biochars present a lower macroporous-mesoporous structure, this fact could be explained in the basis on the better functional groups' structure of the impregnated materials. The presence of NO_3^- and Zn-O oxygenated functional groups on the impregnated materials favors the adsorption in this step, because of the BB attraction effect. Comparing between the impregnated biochars, higher amount of Zn-based compounds on the surface of biochar, affect negatively this process.

3.4 Pb adsorption experiments

3.4.1 Equilibrium adsorption experiments

Pb equilibrium experiment was carried out in a batch reactor, using the produced materials, with a particle size of >0.25 mm, biochar dose of 0.3 g/L, pH = 6, initial Pb concentrations of 10, 20, 50, 100 and 200 mg/L and stirring time of 48 h. Figure 5 shows the fitting curves of the Langmuir, Freundlich and Dubinin-R models for the Pb adsorption equilibrium data with the produced materials. Since y-axis is in the same scale (q_e between 0-300 mg/g) for all materials, it is noticeable the difference in the equilibrium adsorption capacity. The Pb isotherms for the bare biochar and the impregnated biochars do not reach completely adsorption equilibrium. Nevertheless, the q_e values of the latter materials are higher than in the case of the bare biochar (170 mg/g for bare biochar and higher than 250 mg/g in the case

of the impregnated biochars).

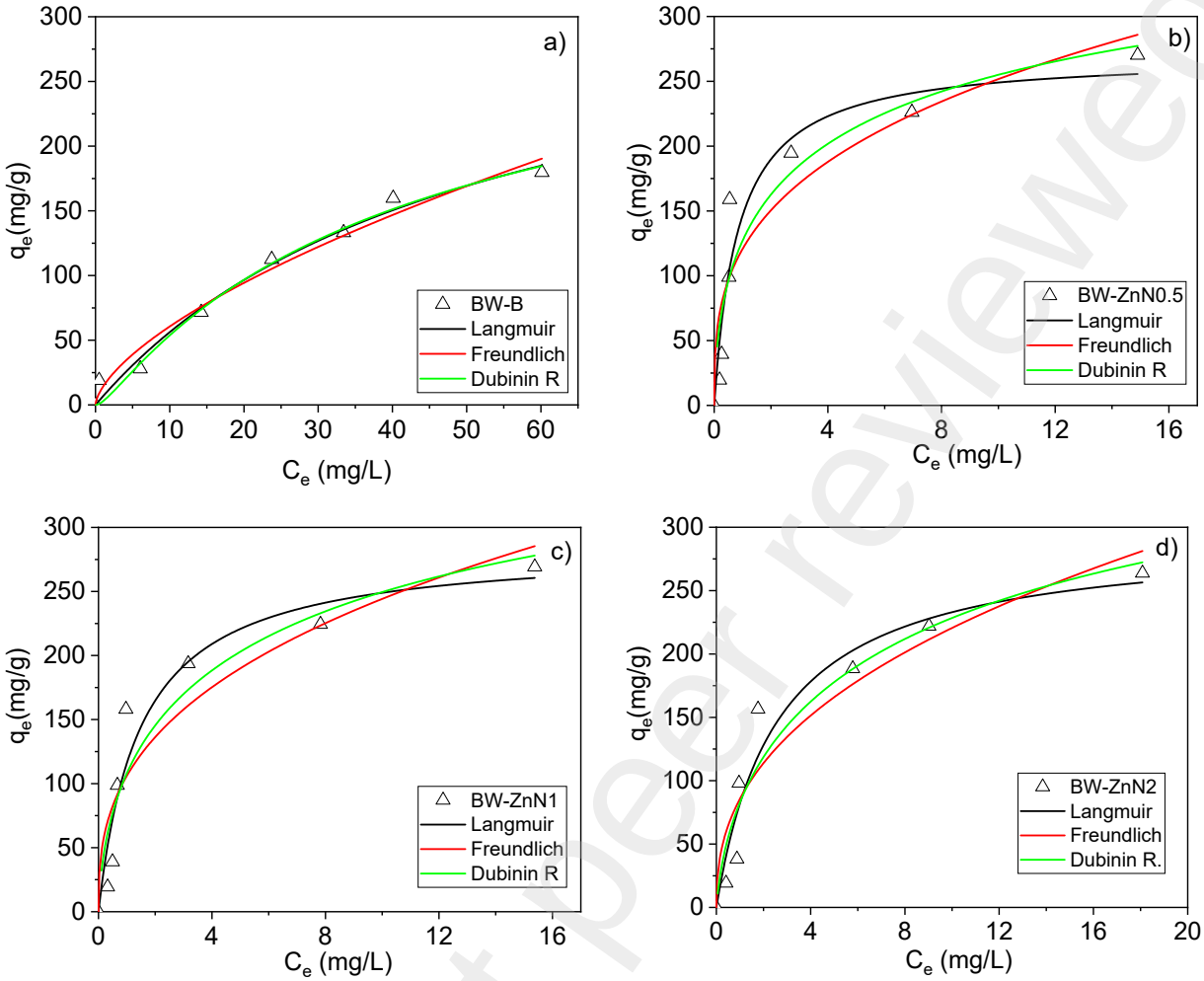

Figure 5. Pb adsorption isotherms (30°C) of the produced materials, BW-B (a), BW-ZnN0.5 (b), BW-ZnN1 (c) and BW-ZnN2 (d).

Table 6 shows the experimental parameters for the applied non-linear models of Langmuir, Freundlich and Dubinin-R on the experimental data. The Langmuir model fits the best to the data of the produced materials according to the comparison of correlation coefficient values and chi-square statistic (X^2). Since the equilibrium state is not clearly reached for all materials, Q_{max} values are overestimated using the Langmuir model and they are not adequate for comparison. Even, in the case of BW-B, the slope of the fitted curve for the Langmuir model is very high at high values of C_e, resulting in an over-dimensioned Q_{max}. Instead of that, the q_e value for the initial concentration of 120 mg/L is used for this aim. When the initial Pb concentration was 120 mg/L, q_e of Pb were 179.73, 270.30, 269.25 and 263.83 mg/g for BW-B, BW-ZnN0.5, BW-ZnN1 and BW-ZnN2, respectively.

Considering the previous fact, the impregnated biochars show higher adsorption capacity than the bare biochar. Additionally, as the precursor concentration increased during impregnation, the Pb adsorption capacity decreases. The better Pb adsorption capacity of the impregnated biochars can be explained by the presence of higher content of oxygenated functional groups compared to the bare biochar.

Table 6. Non-linear models fitted for Pb equilibrium adsorption data.

Models	Parameters	BW-B	BW-ZnN0.5	BW-ZnN1	BW-ZnN2
Langmuir	Q_{max} (mg/g)	340.59	270.09	285.35	292.95
	K_L (L/g)	0.02	1.18	0.68	0.38
	R^2	0.986	0.933	0.937	0.945
	X^2	76.46	808.44	749.81	627.25
Freundlich	K_F (mg/g) /(mg/L)^n	13.95	120.64	106.06	85.66
	N	0.63	0.31	0.36	0.41
	R^2	0.978	0.878	0.879	0.905
	X^2	118.53	1464.42	1443.86	1089.13
Dubinin-Radushkevich	q_{DR}(mg/g)	296.86	381.95	405.40	411.50
	K_{DR} (mol^2/kJ^2)	0.022	0.005	0.006	0.008
	E (kJ/mol)	4.76	10.00	9.12	7.90
	R^2	0.986	0.901	0.909	0.931
	X^2	77.79	1110.25	1078.76	786.78

Analyzing sorption energies (Table 6), calculated by the Dubinin-R model, BW-B shows a lower value than in the case of the impregnated biochar. The value for BW-B is in the range of physical adsorption, while for BW-ZnN0.5, BW-ZnN1 and BW-ZnN2, predominant role of ion-exchange is considered. In the case of the three impregnated materials, as higher the precursor concentration as lower the E value. These facts are consistent with the higher surface functional groups in the impregnated biochars compared to the bare biochar. Analyzing only impregnated materials, the results are in accordance with the larger amounts of impurities when the ZnN concentration increased during the impregnation process.

3.4.2 Kinetic adsorption experiments

Figure 6 shows the Pb adsorption kinetic data of the produced materials collected at Pb initial concentrations (C_i) of 10, 50 and 100 mg/L and material loadings (m) of 0.3 and 0.5 g/L. The adsorption is very fast during the first 10 to 20 min, then it tends to reduce until

the equilibrium is reached. At the initial Pb concentration of 10 mg/L, for both material loadings, the impregnated biochars present clearly better Pb adsorption capacity than the bare biochar. Nevertheless, when the concentration of Pb increased, the adsorption capacity of the bare biochar is closely similar to those for the impregnated materials. Despite the impregnated materials content superior chemical surface properties, the bare biochar still possesses higher surface and pore volume. It seems that the difference in textural properties allows the bare biochar to have almost the same Pb adsorption capacity as the impregnated materials.

Table 7 shows the experimental parameters for the applied nonlinear mathematical pseudo-first order and pseudo-second order models for the Pb adsorption kinetic data of the produced materials. Analyzing R^2 and X^2 of the applied models, almost all materials fit the best to the pseudo-second order model, which could mean that the interaction between adsorbate and adsorbent is chemical in nature. It can by partially supported by the results of adsorption energy for impregnated materials calculated by D-Radushkevich model.

Figure S2 shows the adjustment of the Pb adsorption kinetic data to the intraparticle diffusion models, whereas Figure 6 depicts the parameters of this model. Most of experiments with different initial Pb concentrations and initial material doses present the three steps of the Pb adsorption process proceed according to this model (surface adsorption, intraparticle diffusion and equilibrium adsorption steps). However, in the case of BW-B for the lowest concentration (10 mg/L) only two steps are recognizable. Since this process does not reach the equilibrium, only the surface adsorption step is accomplished and the intraparticle diffusion is in process. Thus, it should be assumed that the high microporous structure of the referred material takes time to be filled and/or the repulsion and attraction forces occur between positively charged Pb^{2+} ions and functional groups on the material surface. This last fact is supported by the positive net surface charge of the material, proved in this study. Despite the net charge of BW-B is negative, the material is amphoteric with positively and negatively charged sites. In the case of impregnated biochars, when the amount of ZnN increased, the pH_{PZC} is reduced, resulting in a reduction in the positiveness of the surface net charge. This fact could favor the adsorption of Pb^{+2} and via a reduction in the repulsion forces with the functional groups of the materials.

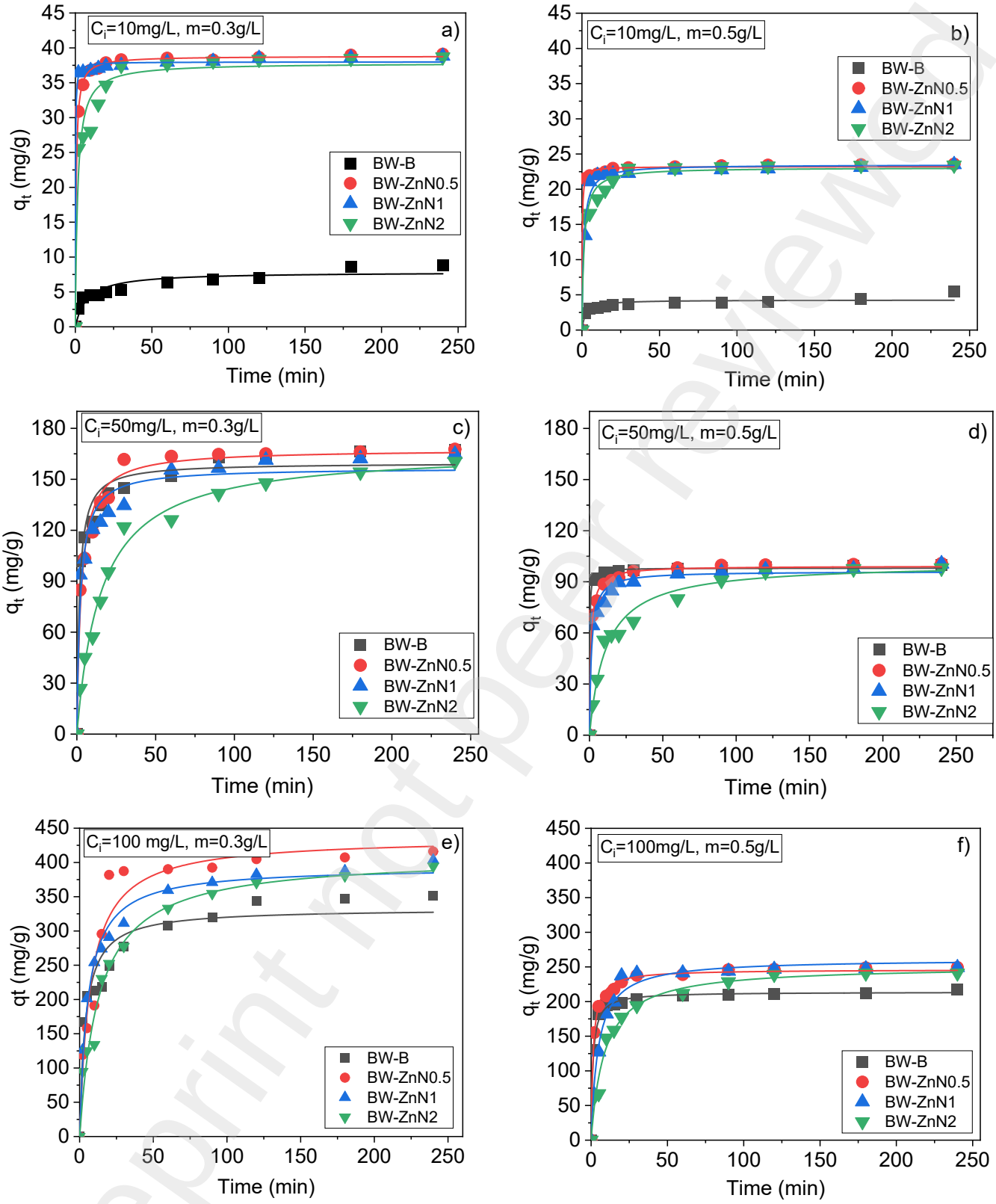

Figure 6. Pb adsorption curves at initial concentration (C_i) of 10, 50 and 100 mg/L and two adsorbent doses (m) 0.3 and 0.5 g/L.

Table 7. Parameters of models fitted for brilliant blue kinetic adsorption data at different initial concentration.

Models	Parameters	BW-B		BW-ZnN0.5		BW-ZnN1		BW-ZnN2	
		0.3 g/L	0.5 g/L	0.3 g/L	0.5 g/L	0.3 g/L	0.5 g/L	0.3 g/L	0.5 g/l
				C_i=10 mg/L					
Pseudo-first order	q_1(mg/g)	7.22	3.96	37.94	22.96	37.71	22.67	35.77	21.95
	k_1(min^{-1})	0.08	0.33	0.80	1.36	1.67	0.46	0.45	0.48
	R^2	0.789	0.802	0.991	0.994	0.996	0.995	0.891	0.914
	X^2	1.42	0.37	1.23	0.29	0.56	0.23	14.51	4.17
Pseudo-second order	q_e (mg/g)	7.84	4.27	38.81	23.21	37.98	23.48	37.83	23.07
	k_2(g/mg.min)	0.016	0.100	0.048	0.217	0.222	0.037	0.017	0.032
	R^2	0.886	0.878	0.999	0.998	0.997	0.985	0.958	0.971
	X^2	0.76	0.23	0.07	0.11	0.33	0.76	5.54	1.39
Intraparticle diffusion	k_{Diff1} (mg/g $min^{-0.5}$)	1.89	1.40	21.8	15.20	25.75	9.43	12.83	11.22
	R_1^2	0.999	0.970	1	1	1	0.999	0.900	1
	k_{Diff2} (mg/g $min^{-0.5}$)	0.37	0.15	3.36	0.44	0.18	0.65	3.42	1.81
	R_2^2	0.980	0.880	0.960	0.960	0.95	0.890	0.950	0.999
	k_{Diff3} (mg/g $min^{-0.5}$)	-	-	0.16	0.05	-	0.12	0.13	0.05
	R_3^2	-	-	0.770	0.960	-	0.970	0.960	0.970
				C_i=50 mg/L					
Pseudo-first order	q_1(mg/g)	150.66	97.03	158.22	95.51	146.53	91.50	148.53	91.50
	k_1(min^{-1})	0.41	1.37	0.21	0.56	0.32	0.47	0.05	0.06
	R^2	0.904	0.995	0.922	0.963	0.873	0.931	0.976	0.945
	X^2	227.30	4.43	210.80	32.28	297.98	58.17	76.03	63.29
Pseudo-second order	q_e (mg/g)	159.64	98.04	167.59	99.25	156.72	96.11	167.51	100.92
	k_2(g/mg.min)	0.004	0.054	0.002	0.010	0.003	0.008	$3.86x10^{-4}$	$8.91x10^{-4}$
	R^2	0.968	0.998	0.979	0.994	0.954	0.981	0.989	0.983
	X^2	75.46	1.63	55.98	5.56	107.52	15.99	35.94	20.25
Intraparticle diffusion	k_{Diff1} (mg/g $min^{-0.5}$)	71.98	64.40	59.96	49.70	66.28	45.5	21.98	16.34
	R_1^2	1	1	1	1	1	1	0.988	0.968
	k_{Diff2} (mg/g $min^{-0.5}$)	6.89	2.08	18.42	6.24	9.48	8.13	4.07	5.76
	R_2^2	0.901	0.913	0.987	0.917	0.962	0.995	0.953	0.991
	k_{Diff3} (mg/g $min^{-0.5}$)	0.80	0.34	0.56	0.42	1.21	0.92	-	0.48
	R_3^2	0.917	0.969	0.981	0.823	0.921	0.909	-	0.924
				Ci=100 mg/L					
Pseudo-first order	q_1(mg/g)	311.60	205.77	405.14	235.25	366.05	245.02	367.89	230.25
	k_1(min^{-1})	0.15	0.47	0.09	0.45	0.11	0.13	0.05	0.08
	R^2	0.814	0.987	0.965	0.961	0.934	0.995	0.961	0.971
	X^2	2075.05	52.56	770.21	214.10	1062.20	38.92	728.55	211.56
Pseudo-second order	q_e (mg/g)	332.64	213.85	436.21	246.23	393.49	261.27	409.11	251.4
	k_2(g/mg.min)	$7.64x10^{-4}$	0.004	$3.17x10^{-4}$	0.003	$4.61x10^{-4}$	$8.36x10^{-4}$	$1.84x10^{-4}$	$4.52x10^{-4}$
	R^2	0.921	0.996	0.954	0.995	0.987	0.984	0.979	0.985
	X^2	875.73	16.85	1029.61	28.72	205.63	123.85	392.31	108.05
Intraparticle diffusion	k_{Diff1} (mg/g $min^{-0.5}$)	94.60	82.50	60.94	88.89	81.77	53.65	56.65	36.81
	R_1^2	0.962	0.991	0.959	0.966	0.990	0.991	0.995	0.969
	k_{Diff2} (mg/g $min^{-0.5}$)	16.6	6.83	145.00	13.48	22.60	1.00	20.85	8.37
	R_2^2	0.957	0.717	0.999	0.990	0.995	0.937	0.982	0.998
	k_{Diff3} (mg/g $min^{-0.5}$)	1.84	1.48	2.99	1.27	5.36	-	6.19	0.42
	R_3^2	0.994	0.879	0.953	0.861	0.968	-	0.968	0.857

3.5 Antimicrobial activity of the produced materials

The antimicrobial activity of the produced materials is demonstrated in Table 7. A positive control, ZnO NPs, was included to further discussion. The bare biochar does not present inhibition capacity against any of the evaluated bacteria. While the impregnated biochars are quite active in this process depending on the bacteria and the initial ZnN concentration

during the impregnation process.

B. firmus was the most susceptible bacteria between the evaluated species. *B firmus* was the only gram-positive bacteria evaluated, while the rest was gram negative. It is well-know that gram-negative bacteria exhibit higher resistant than gram positive, because of resistant mechanism that included production of enzymes, active efflux mechanisms, membrane modification, capsule production, among others [46]. Among Gram-negative bacteria, the order of resistant capacity against the impregnated materials was *E. coli* > *P. vulgaris* > *C. freundii*.

In general, in the case of the impregnated biochars the antibacterial capacity against evaluated bacteria increased with increasing ZnN concentration used during impregnation and increasing dose of the materials (0.04 g present higher antibacterial capacity than 0.02 g).

Comparing the results with the positive control, the inhibition capacity of BW-ZnN2 was comparable or even higher in some cases with that for pure ZnO NPs in both doses, except against *B. firmus*. Comparing with the rest of impregnated materials, the positive control was the best.

The antibacterial capacity of the impregnated biochar is related to the bacterial toxicity of the compounds evolved from ZnN used during the impregnation process. According to the characterization section, different Zn-based compounds, such as residual ZnN, ZHN and ZnO, were detected on the surface of the impregnated biochars. All mentioned compounds are able to release Zn^{2+}, which is a recognized antibacterial agent. Releasing Zn^{2+} could damage bacterial cells via two mechanisms. The first is the interaction with the cell membrane, while the second is based on its penetration through the cell membrane, subsequent protein denaturation and loss of cell proliferation [47]. In the first mechanism, Zn^{2+} is electrostatically attracted by the negative charged membrane cell and its net charge balance is altered, causing deformation and bacteria lysis.

Table 8. Antibacterial activity of banana rachis biochar, composites and ZnO NPs

Bacteria	Diameter of the inhibition zone (mm)									
	BW-B		**BW-ZnN0.5**		**BW-ZnN1**		**BW-ZnN2**		**ZnO NPs**	
	0.02 g	**0.04 g**	**0.02 g**	**0.04 g**	**0.02 g**	**0.04 g**	**0.02 g**	**0.04 g**	**0.02 g**	**0.04 g**
P. vulgaris	0	0	0	0	0	11.6±0.11	10.2±0.12	11.7±0.05	11.7±0.11	15.6±0.41
C. freundii	0	0	0	7±0.12	0	7±0.08	9±0.13	13.9±0.29	8.6±0.12	11±0.26
E. coli	0	0	0	0	0	0	9.3±0.09	29±1.68	10±0.07	12.2±0.18
B. firmus	0	0	5±0.09	12.9±0.09	5±0.11	44.1±0.08	16.7±0.27	24.3±1.12	23.3±0.55	44.7±0.84

4.- Conclusions

Banana rachis-based biochar was successfully impregnated with different concentrations of zinc nitrate hexahydrate (0.5, 1 and 2 M) using proposed method. Zn-containing compounds, such as residual ZnN, ZHN and/or ZnO, mostly in the crystalline phase, were deposited on the biochar surface, incorporating surface functional groups such as NO_3^- and Zn-O. When the lowest initial precursor concentration was used, ZnN is predominant in the crystalline phase, while when the concentration of the precursor increased ZHN was the major Zn-containing admixture.

The impregnation of biochar negatively affects the structural properties, however the incorporation of oxygenated surface functional groups increased Pb and BB adsorption capacities of the impregnated materials compared to the bare biochar. However, comparing to the impregnated biochars, the increased precursor concentration causes a reduction in the adsorption capacity because of the obstruction of microporosity by Zn-based compounds formed during the impregnation process.

The impregnation increases the antibacterial capacity of biochar against bacteria such as Gram-negative *E. coli*, *P. vulgaris* and *C. freundii;* and Gram-positive *B. firmus*. The antibacterial capacity improves with the increased precursor concentration, and it is based on Zn^{2+} releasing. Impregnation of biochar with ZnN using post-impregnation mild temperature conditions enhances the adsorption and antibacterial capacities. Nevertheless, further studies should be carried out with other kinds of pollutants.

5.- Acknowledgement

This work received financial support from National Council for Science, Technology and Technological Innovation (CONCYTEC) and the National Program for Scientific Research and Advanced Studies (PROCIENCIA) within the framework of the competition E072-2024-01-BM “Projects for Needs of Strategic Areas Based on Challenges” Grant number PE501093763-2024.

Part of the experimental results were accomplished using Large Research Infrastructure ENREGAT supported by the Ministry of Education, Youth and Sports of the Czech Republic (projects No. LM2018098 and No. LM2023056). L. Matějová also thanks the financial support of the European Union under the REFRESH - Research Excellence For Region Sustainability and High-tech Industries, project no. CZ.10.03.01/00/22_003/0000048, via the Operational Programme Just Transition. XPS

measurements were carried out with the equipment purchased thanks to the financial support of the European Regional Development Fund in the framework of the Polish Innovation Economy Operational Program (contract no. POIG.02.01.00-12-023/08). The research has been supported by a grant from the Faculty of Chemistry under the Strategic Programme Excellence Initiative at Jagiellonian University.

6.- References

[1] J.F. Cruz, G.J.F. Cruz, K. Ainassaari, M.M. Gómez, J.L. Solís, R.L. Keiski, Microporous activation carbon made of sawdust from two forestry species for adsorption of methylene blue and heavy metals in aqueous system – case of real polluted water, Revista Mexicana de Ingeniería Química, 17 (2018) 847-861.
[2] B.G. Marshall, M.M. Veiga, R.J. Kaplan, R. Adler Miserendino, G. Schudel, B.A. Bergquist, J.R.D. Guimaraes, L.G.S. Sobral, C. Gonzalez-Mueller, Evidence of transboundary mercury and other pollutants in the Puyango-Tumbes River basin, Ecuador-Peru, Environ Sci Process Impacts, 20 (2018) 632-641.
[3] M. Pirilä, G.J.F. Cruz, K. Ainassaari, M.M. Gomez, L. Matějová, R.L. Keiski, Adsorption of As (V), Cd (II) and Pb (II), in Multicomponent Aqueous Systems using Activated Carbons, Water Environment Research, 89 (2017) 846-855.
[4] D. Mondal, R. Periche, B. Tineo, L.A. Bermejo, M.M. Rahman, A.B. Siddique, M.A. Rahman, J.L. Solis, G.J.F. Cruz, Arsenic in Peruvian rice cultivated in the major rice growing region of Tumbes river basin, Chemosphere, 241 (2020) 125070.
[5] A.M. Mora, D. Jumbo-Flores, M. González-Merizalde, S.A. Bermeo-Flores, Niveles De Metales Pesados En Sedimentos De La Cuenca Del RÍo Puyango, Ecuador, Revista Internacional de Contaminación Ambiental, 32 (2016) 385-397.
[6] B.G. Marshall, M.M. Veiga, R.J. Kaplan, R. Adler Miserendino, G. Schudel, B.A. Bergquist, J.R.D. Guimarães, L.G.S. Sobral, C. Gonzalez-Mueller, Evidence of transboundary mercury and other pollutants in the Puyango-Tumbes River basin, Ecuador–Peru, Environmental Science: Processes & Impacts, 20 (2018) 632-641.
[7] A. Kumar, A. Kumar, C.-P. MMS, A.K. Chaturvedi, A.A. Shabnam, G. Subrahmanyam, R. Mondal, D.K. Gupta, S.K. Malyan, S.S. Kumar, Lead toxicity: health hazards, influence on food chain, and sustainable remediation approaches, International journal of environmental research and public health, 17 (2020) 2179.
[8] H.B. Slama, A. Chenari Bouket, Z. Pourhassan, F.N. Alenezi, A. Silini, H. Cherif-Silini, T. Oszako, L. Luptakova, P. Golińska, L. Belbahri, Diversity of synthetic dyes from textile industries, discharge impacts and treatment methods, Applied Sciences, 11 (2021) 6255.
[9] A. Gičević, L. Hindija, A. Karačić, Toxicity of azo dyes in pharmaceutical industry, in: CMBEBIH 2019: Proceedings of the International Conference on Medical and Biological Engineering, 16 18 May 2019, Banja Luka, Bosnia and Herzegovina, Springer, 2020, pp. 581-587.
[10] S. Sartaj, N. Ali, A. Khan, S. Malik, M. Bilal, M. Khan, N. Ali, S. Hussain, H. Khan, S. Khan, Performance evaluation of photolytic and electrochemical oxidation processes for enhanced degradation of food dyes laden wastewater, Water Science and Technology, 81 (2020) 971-984.
[11] A. Ahmad, M. Priyadarshini, S. Yadav, M.M. Ghangrekar, R.Y. Surampalli, Evaluation of waste medicine wrappers as an efficacious low-cost novel electrode material in electrocoagulation for the remediation of Coomassie Brilliant Blue from wastewater, Journal of Environmental Chemical Engineering, 11 (2023) 110484.
[12] M.G. Gonçalves, P.A. da Silva Veiga, M.R. Fornari, P. Peralta-Zamora, A.S. Mangrich, S. Silvestri, Relationship of the physicochemical properties of novel ZnO/biochar composites to their efficiencies in the degradation of sulfamethoxazole and methyl orange, Science of The Total

Environment, 748 (2020) 141381.
[13] X. Tan, Y. Liu, G. Zeng, X. Wang, X. Hu, Y. Gu, Z. Yang, Application of biochar for the removal of pollutants from aqueous solutions, Chemosphere, 125 (2015) 70-85.
[14] G.J. Cruz, D. Mondal, J. Rimaycuna, K. Soukup, M.M. Gómez, J.L. Solis, J. Lang, Agrowaste derived biochars impregnated with ZnO for removal of arsenic and lead in water, Journal of Environmental Chemical Engineering, 8 (2020) 103800.
[15] A. Nakarmi, S.E. Bourdo, L. Ruhl, S. Kanel, M. Nadagouda, P. Kumar Alla, I. Pavel, T. Viswanathan, Benign zinc oxide betaine-modified biochar nanocomposites for phosphate removal from aqueous solutions, Journal of Environmental Management, 272 (2020) 111048.
[16] M.A. Albo Hay Allah, H.K. Ibrahim, H.A. Alshamsi, H. Radhi Saud, Eco-friendly synthesis of biochar supported with zinc oxide as a heterogeneous catalyst for photocatalytic decontamination of Rhodamine B under sunlight illumination, Journal of Photochemistry and Photobiology A: Chemistry, 449 (2024) 115413.
[17] J. Wu, T. Wang, N. Shi, F. Min, W.P. Pan, Hierarchically porous biochar templated by in situ formed ZnO for rapid Pb(2+) and Cd(2+) adsorption in wastewater: Experiment and molecular dynamics study, Environ Pollut, 302 (2022) 119107.
[18] Y. Guo, X. Liu, S. Xie, H. Liu, C. Wang, L. Wang, 3D ZnO modified biochar-based hydrogels for removing U(VI) in aqueous solution, Colloids and Surfaces A: Physicochemical and Engineering Aspects, 642 (2022) 128606.
[19] Z. Alves, P. Brites, N.M. Ferreira, G. Figueiredo, G. Otero-Irurueta, I. Gonçalves, S. Mendo, P. Ferreira, C. Nunes, Thermoplastic starch-based films loaded with biochar-ZnO particles for active food packaging, Journal of Food Engineering, 361 (2024) 111741.
[20] Mankomal, H. Kaur, Synergistic effect of biochar impregnated with ZnO nano-flowers for effective removal of organic pollutants from wastewater, Applied Surface Science Advances, 12 (2022) 100339.
[21] Z. Alves, N.M. Ferreira, G. Figueiredo, S. Mendo, C. Nunes, P. Ferreira, Electrically conductive and antimicrobial agro-food waste biochar functionalized with zinc oxide particles, International Journal of Molecular Sciences, 23 (2022) 8022.
[22] V.R. Venu Gopal, S. Kamila, Effect of temperature on the morphology of ZnO nanoparticles: a comparative study, Applied Nanoscience, 7 (2017) 75-82.
[23] N. Sedefoglu, Green synthesis of ZnO nanoparticles by Myrtus communis plant extract with investigation of effect of precursor, calcination temperature and study of photocatalytic performance, Ceramics International, 50 (2024) 9884-9895.
[24] A. Joseph Anthuvan, K. Kumaravel, V. Chinnuswamy, Synergetic effect of hierarchical zinc oxide (ZnO) nanostructure with enhanced adsorption and antibacterial action towards waterborne detrimental contaminants, Applied Nanoscience, 11 (2021) 2181-2198.
[25] J. Lang, L. Matějová, A.K. Cuentas-Gallegos, D.R. Lobato-Peralta, K. Ainassaari, M.M. Gómez, J.L. Solís, D. Mondal, R.L. Keiski, G.J.F. Cruz, Evaluation and selection of biochars and hydrochars derived from agricultural wastes for the use as adsorbent and energy storage materials, Journal of Environmental Chemical Engineering, 9 (2021) 105979.
[26] ASTM, Standard Test Methods for Moisture in Activated Carbon, in: Standard Test Methods, West Conshohocken, 2004.
[27] ASTM, Standard Test Method for Total Ash Content of Activated Carbon, in: Standard Test Method, ASTM International, West Conshohocken, 2004.
[28] L. Román, D. Maurtua, F. Paraguay-Delgado, J.L. Solís, M.M. Gómez, Green Synthesis of ZnO_2 Nanoparticles and Their Annealing Transformation Into ZnO Nanoparticles: Characterization and Antimicrobial Activity, Journal of Nanoscience Nanotechnology, 16 (2016) 9889-9895.
[29] A.M. Dehkhoda, N. Ellis, E. Gyenge, Electrosorption on activated biochar: effect of thermo-chemical activation treatment on the electric double layer capacitance, Journal of Applied Electrochemistry, 44 (2013) 141-157.
[30] M. Smith, L. Scudiero, J. Espinal, J.-S. McEwen, M. Garcia-Perez, Improving the deconvolution and interpretation of XPS spectra from chars by ab initio calculations, Carbon, 110 (2016) 155-171.

[31] L. Dake, D. Baer, J. Zachara, Auger parameter measurements of zinc compounds relevant to zinc transport in the environment, Surface and Interface analysis, 14 (1989) 71-75.
[32] H. Cai, D. Zhang, X. Ma, Z. Ma, A novel ZnO/biochar composite catalysts for visible light degradation of metronidazole, Separation and Purification Technology, 288 (2022) 120633.
[33] Z. Alves, N.M. Ferreira, G. Figueiredo, S. Mendo, C. Nunes, P. Ferreira, Electrically Conductive and Antimicrobial Agro-Food Waste Biochar Functionalized with Zinc Oxide Particles, Int J Mol Sci, 23 (2022).
[34] T. Galya, V. Sedlarik, I. Kuritka, J. Sedlarikova, P. Saha, Characterization of Antibacterial Polymeric Films Based on Poly(vinyl alcohol) and Zinc Nitrate for Biomedical Applications, International Journal of Polymer Analysis and Characterization, 13 (2008) 241-253.
[35] N.F. Khadiran, M.Z. Hussein, R. Ahmad, T. Khadiran, Z. Zainal, W.R.W.A. Kadir, S.S. Hashim, Preparation and properties of zinc layered hydroxide with nitrate and phosphate as the counter anion, a novel control release fertilizer formulation, Journal of Porous Materials, 28 (2021) 1797-1811.
[36] E. Turianicová, M. Kaňuchová, A. Zorkovská, M. Holub, Z. Bujňáková, E. Dutková, M. Baláž, L. Findoráková, M. Balintová, A. Obut, CO2 utilization for fast preparation of nanocrystalline hydrozincite, Journal of CO2 Utilization, 16 (2016) 328-335.
[37] N. Strutynska, O. Livitska, S. Prylutska, Y. Yumyna, P. Zelena, L. Skivka, A. Malyshenko, L. Vovchenko, V. Strelchuk, Y. Prylutskyy, N. Slobodyanik, U. Ritter, New nanostructured apatite-type (Na+,Zn2+,CO32−)-doped calcium phosphates: Preparation, mechanical properties and antibacterial activity, Journal of Molecular Structure, 1222 (2020) 128932.
[38] P. Li, L. Li, Y. Du, M.A. Hampton, A.V. Nguyen, L. Huang, V. Rudolph, Z.P. Xu, Potential foliar fertilizers with copper and zinc dual micronutrients in nanocrystal suspension, Journal of Nanoparticle Research, 16 (2014) 2669.
[39] P. Li, Z.P. Xu, M.A. Hampton, D.T. Vu, L. Huang, V. Rudolph, A.V. Nguyen, Control Preparation of Zinc Hydroxide Nitrate Nanocrystals and Examination of the Chemical and Structural Stability, The Journal of Physical Chemistry C, 116 (2012) 10325-10332.
[40] S. Noohi, H. Asadian, Application of FTIR microscopy to identify some glass plates of golestan palace photo archive, Iranian Conservation Science Journal, 1 (2017) 48-53.
[41] H. Jing, L. Ji, Z. Wang, J. Guo, S. Lu, J. Sun, L. Cai, Y. Wang, Synthesis of ZnO Nanoparticles Loaded on Biochar Derived from Spartina alterniflora with Superior Photocatalytic Degradation Performance, Nanomaterials (Basel), 11 (2021) 2479.
[42] H. Roy, M.S. Islam, M.T. Arifin, S.H. Firoz, Synthesis, Characterization and Sorption Properties of Biochar, Chitosan and ZnO-Based Binary Composites towards a Cationic Dye, Sustainability, 14 (2022) 14571.
[43] M. Thommes, K. Kaneko, A.V. Neimark, J.P. Olivier, F. Rodriguez-Reinoso, J. Rouquerol, K.S.W. Sing, Physisorption of gases, with special reference to the evaluation of surface area and pore size distribution (IUPAC Technical Report) %J Pure and Applied Chemistry, 87 (2015) 1051.
[44] H.N. Tran, S.-J. You, A. Hosseini-Bandegharaei, H.-P. Chao, Mistakes and inconsistencies regarding adsorption of contaminants from aqueous solutions: A critical review, Water Research, 120 (2017) 88-116.
[45] H. Tamai, T. Yoshida, M. Sasaki, H. Yasuda, Dye adsorption on mesoporous activated carbon fiber obtained from pitch containing yttrium complex, Carbon, 37 (1999) 983-989.
[46] J.A. Lepe, L. Martínez-Martínez, Resistance mechanisms in Gram-negative bacteria, Medicina Intensiva (English Edition), 46 (2022) 392-402.
[47] S. Jiang, K. Lin, M. Cai, ZnO Nanomaterials: Current Advancements in Antibacterial Mechanisms and Applications, Frontiers in Chemistry, 8 (2020) 580.